Ultramicroscopy 000 (2017) 1–9

Contents lists available at ScienceDirect

Ultramicroscopy

journal homepage: www.elsevier.com/locate/ultramic

Perspectives on in situ electron microscopy

Haimei Zheng[a,b,*], Yimei Zhu[c,d]

[a] Materials Sciences Division, Lawrence Berkeley National Laboratory, Berkeley, CA 94720, USA
[b] Department of Materials Science and Engineering, University of California, Berkeley, CA 94720, USA
[c] Department of Condensed Matter Physics and Materials Science, Brookhaven National Laboratory, Upton, NY 11973, USA
[d] Department of Physics and Astronomy, Stony Brook University, Stony Brook, NY 11790, USA

ARTICLE INFO

Article history:
Received 8 November 2016
Revised 12 March 2017
Accepted 18 March 2017
Available online xxx

Keywords:
In situ TEM
Liquid cell TEM
Aberration correction
Colloidal nanocrystal growth
Ferroelectric vortices
Ferromagnetic domains switching

ABSTRACT

In situ transmission electron microscopy (TEM) with the ability to reveal materials dynamic processes with high spatial and temporal resolution has attracted significant interest. The recent advances in in situ methods, including liquid and gas sample environment, pump-probe ultrafast microscopy, nanomechanics and ferroelectric domain switching the aberration corrected electron optics as well as fast electron detector has opened new opportunities to extend the impact of in situ TEM in broad areas of research ranging from materials science to chemistry, physics and biology. In this article, we highlight the development of liquid environment electron microscopy and its applications in the study of colloidal nanoparticle growth, electrochemical processes and others; in situ study of topological vortices in ferroelectric and ferromagnetic materials. At the end, perspectives of future in situ TEM are provided.

1. Introduction

In situ electron microscopy has been identified as one of the major future directions of electron microscopy (BES workshop report [1]). It provides the opportunity to observe at the atomic level materials responses to an external stimulus, discover transient states during chemical or structural transformations, and correlate materials structure to their functionalities [2–5]. There are many fascinating research topics using in situ transmission electron microscopy (TEM) owing to the advances of in situ methods, ranging from liquid and gas environment TEM [3,4] to pump-probe ultrafast microscopy [6-8], nanomechanics [9,10] and ferroelectric domain switching [11,12]. With the advances in electron microscopy, it has been possible to achieve 0.5 Å spatial resolution using an aberration corrected TEM [13], high speed data acquisition (~2.5 ms or better) with a fast camera [14] and electron energy loss spectroscopy (EELS) enables the study of spin waves with an energy resolution down 1 or 2 meV [15]. Many of these advances can be attributed to the earlier critical contribution from Dr. Ondrej Krivanek [16-18]. For in situ measurements, it is often a challenge to achieve the best performance of an aberration corrected microscope due to an unideal thick sample, sample vibration in chemical reactions or under an external stimulus, insufficient electron flux during fast data acquisition and so on. However, it is clear that with the advances in electron microscopy including the aberration corrected TEM, EDS with large collection angle, fast and sensitive electron detection, large data processing, in situ electron microscopy has become increasingly powerful and popular. There is no doubt in situ TEM will bring significant impact in broad areas of research from materials science to physics, chemistry and biology.

In this article, a few recent in situ TEM work in the area of *materials chemistry*, such as colloidal nanoparticle growth and electrochemical processes using liquid environmental cells, and in *solid state physics*, such as topological vortices in ferroelectric and ferromagnetic materials, ferroelectric or ferromagnetic domain switching are highlighted. We hope this article can help to provide a view on the broad applications of in situ TEM. At the end, conclusion and an outlook into future challenges and opportunities in in situ TEM including the impact of aberration corrected TEM and fast electron detection are provided.

The development of liquid cells has opened many opportunities for the study of materials dynamic processes in liquids with TEM, such as, nucleation and growth, self-assembly of nanomaterials, electrochemical processes, biological materials in physiological conditions, etc. In the past a few years, publications on the topic of liquid cell TEM study have increased rapidly [4]. Here, we review a few recent studies on nanoparticle growth in a liquid cell with atomic resolution imaging and high temporal resolution (400 frames per second), the in situ lithiation/delithation of MoS_2 nanoflakes in an electrochemical cell with EDS and nanobeam

* Corresponding author.
E-mail addresses: hmzheng@lbl.gov, zhu@bnl.gov (H. Zheng).

http://dx.doi.org/10.1016/j.ultramic.2017.03.022
0304-3991/

diffraction, which highlight the growing impact of in situ liquid environmental electron microscopy in materials chemistry and chemical research.

In the second part of this paper, a couple of examples on in situ electron microscopy of ferroelectric or ferromagnetic vortexes and domain switching are provided. There has been significant recent interest on topological phase transitions and topological phases of matter. Topological structures, emerging near spontaneous symmetry-breaking transitions, are ubiquitously observed in wide branches of science [19-22]. In condensed matter, topological defects can be promising candidates for information storage technology. Skyrmions, multiferroic vortices, domain walls, dislocations, and disclinations are examples, where emergent properties and behaviors have been reported [23-28]. These topological defects are invariant under continuous deformations or perturbations, and thus said to be protected by topology. They often are observable and play important roles in phase transition. Their fascinating underlying physics responsible for striking geometric patterns can be found in order parameter space [29]. In situ TEM is a unique approach to topological structures, where the aberration corrected electron microscopy plays a major role.

2. In situ TEM study of materials dynamics in liquids

Most liquids including water and other organic solvent have a high vapor pressure, thus they are incompatible with the high vacuum environment of a transmission electron microscope. To separate the liquid samples from the vacuum environment, a sealed liquid cell is required. A liquid cell needs a thin imaging window allowing electron beam to go through while being able to survive in high vacuum. The concept of windowed TEM cell was introduced in the early days of electron microscopy. From the earliest attempt of imaging wet samples using sandwiched thin aluminum foils in 1930s [30] to the liquid cells nowadays with thin SiNx/Si membrane [31,32] or graphene liquid cell [33] or electrochemical cells allowing an applied electric bias [34], tremendous progress has been made and breakthrough discoveries have been achieved.

The self-contained liquid cells with ultra-thin SiNx membrane (as thin as 10 nm [32]) or graphene offer superb atomic image resolution [33]. SiNx membranes are mechanically strong, inert, with low imaging contrast thus excellent for electrochemical cells. Various types of patterned electrodes (e.g., Au, Ti, Al, Pt, graphene, etc.) can be made into an electrochemical liquid cell with SiNx membranes. It is also possible to flow liquids between the two silicon nitride membranes of a liquid cell using external tubing and a syringe pump, which has been widely used in a commercial liquid cell stage and is attractive for the study of reactions with instant mixing of liquids.

Liquid cell TEM has been used for the exploration of new frontiers for materials synthesis, electrochemistry, catalysis, fluid physics, biological materials in aqueous environments and many other areas of research [3]. Compared to many other in situ approaches, such as in situ optical spectroscopy, [35] x-ray spectroscopic methods, [36-40] atomic force microscopy (AFM) and scanning tunneling microscopy (STM), [41-43] in situ TEM has its unique advantages allowing directly observation of materials transformation dynamics in liquids with high spatial down to the atomic range and high temporal resolution in millisecond. The major criticisms come from the electron beam radiation damage and the challenges in controlling of local environment, reactant mixing, etc. during reactions, which will also be discussed in this article.

2.1. Liquid cell TEM study of colloidal nanocrystal growth

Crystallization process in colloidal solution is complex involving the arrangement of thousands of atoms and molecules near the surface, and it is further complicated by the interactions between atoms and the environment changes [44]. With modifications of the temperature, precursor and surfactants, it is possible to make various nanocrystals with certain size and shape, on which there have been many studies [45,46]. Liquid cell TEM is a unique method to study nanocrystal growth mechanisms by revealing single nanoparticle trajectories and elucidating the role of different factors in controlling structure and morphology of a nanoparticle [4].

Here, we show a series of successful studies on nanoparticle shape evolution to highlight the significant progress that has been made on liquid cell TEM owing to the liquid cell development and the advances in electron microscopy and fast electron detection. For example, in colloidal nanocrystal synthesis, it is often assumed that in order to achieve monodisperse nanoparticles coalescence between nanoparticles should be avoided. It was reported by Zheng et al. [47] that with real time liquid cell TEM, observations reveal two types of growth, either by monomer attachment or by coalescence, leading to the same particle size (Fig. 1a) [47]. Fascinating growth by nanoparticle attachment has also been observed in Pt-Fe nanowire formation [14]. The interactions between Pt-Fe nanoparticles result in nanoparticle end-to-end attachment into a chain (Fig. 1b). Further systematic liquid cell TEM studies by changing the surfactant concentration have been carried out and the results have demonstrated that surfactants can drastically influence morphology of a nanoparticle, modify the growth rate of certain facets, inhibit nanoparticle aggregation, and prevent coalescence [44].

Another example is on in situ high resolution imaging of Pt nanocrystal growth and shape evolution with liquid cell TEM [32]. Wulff construction [48,49] has been used to predict the equilibrium shape of nanocrystals, where it states that the growth rate of certain facet is proportional to the surface free energy. For the growth of nanocrystals the high-energy facet grows at a higher rate than the low-energy facets, therefore, the fast growing facets will eventually disappear resulting in a nanocrystal terminated with low energy facets [50,51]. It was assumed that the commonly used surfactants modify the energy of specific facets through preferential adsorption, influencing the relative growth rate of different facets thus the shape of a nanocrystal [52,53]. However, in situ observations of Pt nanocube formation using liquid cell TEM show drastic deviation from the Wulff construction prediction [32]. As shown in Fig. 1c and d, we found the growth rates of all low index facets, {1 0 0}, {1 1 0} and {1 1 1}, are similar until the {1 0 0} facets stop growing. The {1 1 0} facets will continue to grow until they reach a limit, at which point they form an edge of a nanocube. The continued growth of {1 1 1} facets fills the corners of the cube. Such atomic facet development in platinum nanocube growth suggests the surface energy minimization rules breaks down at the nanoscale. Density functional theory (DFT) calculation reveals that the drastic differences of ligands mobility on different facets, i.e., ligands move several orders of magnitude slower on {1 0 0} than {1 1 1} facets retarded the growth of {1 0 0} facets. Therefore, a selective facet arrested shape control mechanisms is proposed. The improved liquid cells with thinner SiNx membranes and a fast electron detector with high detection quantum efficiency (Gatan K2 IS camera) are critical for achieving high spatial resolution at the atomic level.

In addition, graphene liquid cells with reduced background noise offer unprecedented resolution (Fig. 2). Park et al. used an aberration-corrected TEM and direct electron detector to resolve the growth and 3D atomic structures of Pt nanocrystals in a graphene liquid cell [33,54]. The observation revealed that Pt nanoparticle coalescence is site-selective and the {1 1 1} facets with lowest surface energy or lowest ligand coverage are preferred for nanoparticle attachment [54].

Please cite this article as: H. Zheng, Y. Zhu, Perspectives on in situ electron microscopy, Ultramicroscopy (2017), http://dx.doi.org/10.1016/j.ultramic.2017.03.022

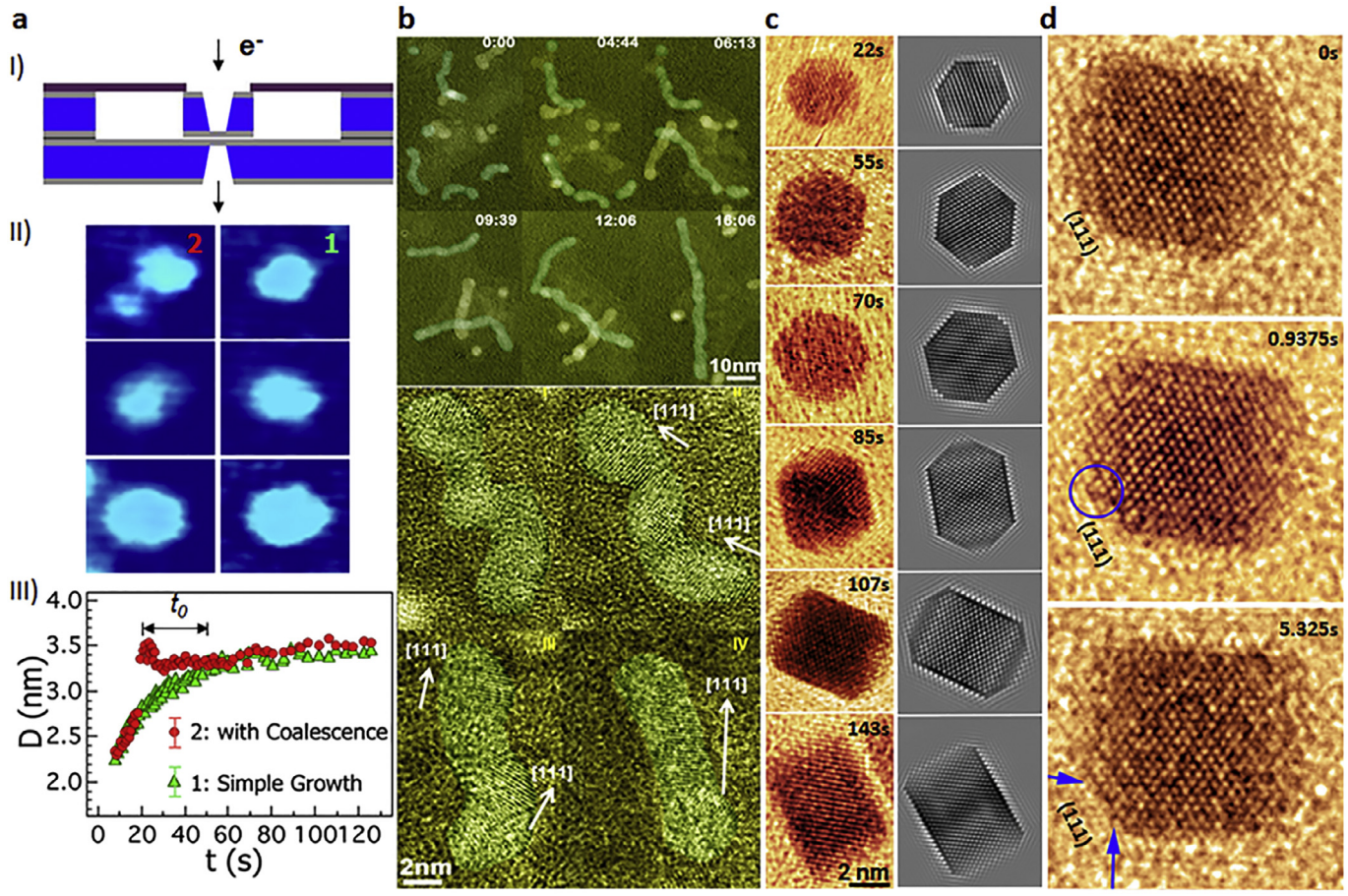

Fig. 1. Single nanoparticle growth trajectories studied using liquid cell TEM. (a) (I) A liquid cell design. (II) Sequential images showing platinum nanoparticle growth either by monomer attachment or by nanoparticle coalescence, leading to the same particle size. (III) Growth trajectories of nanoparticles shown in (II) [31]. (b) Pt-Fe nanocrystal growth and attachment to form nanowires. Random attachment and recrystallization to form a single crystal nanowire [14]. (c) Facet development during Pt nanocube growth. (d) (left) sequential high resolution TEM images of the growth of (1 1 1) facet. A cluster of atoms formed on the facet and it was subsequently transformed into a monolayer. (right) the atomic growth of (1 1 0) facet [32].

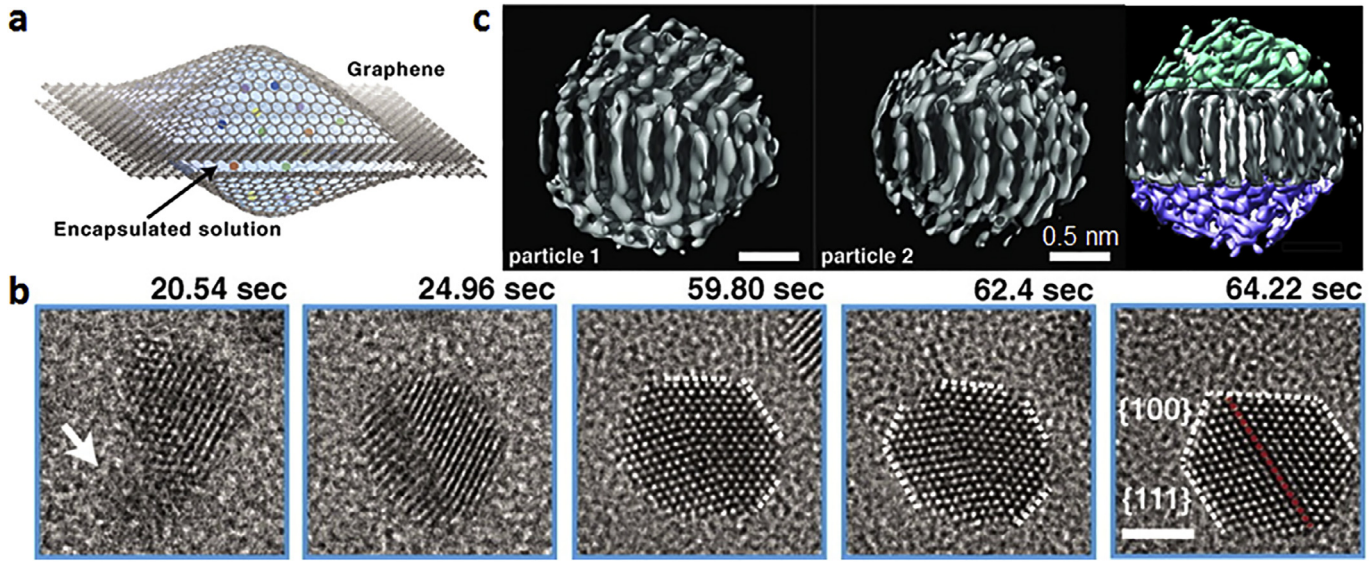

Fig. 2. Nanocyrstal dynamics observed in a graphene liquid cell. (a) A graphene liquid cell schematic. (b) Sequential images showing Pt nanocrystal formation with atomic resolution. (c) Two Pt nanocrystals from a graphene liquid cell after 3D reconstruction. Colors on the right correspond to defects (twins) in one particle [33]. (For interpretation of the references to color in this figure legend, the reader is referred to the web version of this article.).

Please cite this article as: H. Zheng, Y. Zhu, Perspectives on in situ electron microscopy, Ultramicroscopy (2017), http://dx.doi.org/10.1016/j.ultramic.2017.03.022

So far, most in situ TEM studies of colloidal nanoparticle growth in a liquid cell use electron beam to trigger the reactions. However, it is often unclear what is the exact role of electron beam in nanocrystal growth. First of all, electron beam induced temperature rise in a liquid cell does not appear to be significant (i.e., a few degrees [47]), thus thermal heating should not be the controlling factor for the electron beam induced nanoparticle growth. Second, the secondary electrons generated from the scattering of primary electrons may reduce metal ions to form metal nanoparticles [31]. However, since complex precursor solution reactions may occur under the electron beam irradiation, electron beam induced nanoparticle growth is much more complex than simple electron reduction reaction. For instance, Liang et al. reported complex transition metal oxide nanoparticle growth in a liquid cell [55]. There have been studies focusing on electron beam induced growth mechanisms [56,57]. However, because different solvent and precursor may react differently to the electron beam, there might not be a universal rule. Direct measurements of the reaction products are necessary to elucidate electron beam induced nanocrystal growth mechanisms. Third, in many cases electron beam effects need to be limited. For instance, avoid electron beam damage is crucial for the study of electrochemical processes using liquid cell TEM as shown in the following session. Nanocrystal growth in a liquid cell induced by thermal heating has also been reported [58]. Colloidal nanocrystal growth in a liquid cell using thermal heating rather than electron beam irradiation could be more straightforward for direct comparison with flask synthesis.

2.2. Electrochemical process induced materials degradation

An electrochemical reaction can be visualized with TEM using a liquid cell where electrodes are built inside the liquid cell. Electrochemical lithiation of Au electrode [59], dendritic growth of lead [60], lithium [34] magnesium [61] and the subsequent stripping of electrodeposited materials have been observed using an electrochemical liquid cell. In addition, in situ study of the solid electrolyte interfaces (SEI) formation in an electrochemical liquid cell has been achieved [62]. Characterization of SEI layer with advanced electron microscopy shows LiF nanoparticles uniformly distributed within the SEI film [34,62].

The fabricated nanobattery cells for TEM offer the opportunity to study the reaction mechanisms of MoS_2 during battery operation. A nanobattery cell with commercial electrolyte $LiPF_6$/EC/DEC for Li ion batteries was used to study structure changes of MoS_2 nanoflakes after lithiation/delithiation. In the nanobattery cell, Li metal was loaded on one electrode as counter (and reference) electrode.

Layered MoS_2 is an attractive electrode material for lithium ion batteries [63,64]. When lithium ions are inserted between the layers of MoS_2, the MoS_2 structure can be exfoliated by ultrasonication of lithiated MoS_2 in H_2O [65,66]. Electrochemical degradation may be induced by the active material loss when MoS_2 is used as the cathode material [67]. In situ observation of lithiation and delithiation of MoS_2 as the electrode material provides critical insight on the degradation mechanisms of this material for battery applications.

Dissolution and lithiation induced deformation of MoS_2 during charge in the voltage range of 1.8–1.2 V were captured in situ. Irreversible decomposition near 1.1 V was observed, where MoS_2 nanosheets broke down into 5–10 nm MoS_2 nanoparticles as confirmed by nanobeam diffraction experiments (Fig. 3). Some MoS_2 nanosheets decompose upon lithiation while the other remain and experience structural changes, i.e., swelling or deformation. The variation of MoS_2 nanosheets during lithiation may result from the MoS_2 thickness difference or inhomogeneity during lithiation. Out in situ study of MoS_2 decomposition during lithiation in battery operation provides insights on improving the battery design and applications of transition metal dichalcogenides (TMDCs) and layered structured materials in energy devices.

For in situ liquid cell TEM study of electrochemical processes, limiting electron beam effects is critical. An effective strategy is to reduce electron beam current (thus, the net electron dosage on the sample). For example, under an electron beam current of 2–10 $e^-/Å^2$ s or below, no reaction was observed without an applied bias [60]. However, the consequence of significantly reducing electron beam current is that spatial resolution is reduced. So far, resolution better than 1 nm in the imaging of a dynamic electrochemical process has not been achieved. Future implementing high sensitive electron detector and lose dose image processing would assist to achieve better resolution.

3. In situ study of topological vortices in ferroelectric and ferromagnetic materials

Understanding topological structures is crucial to the prediction of behavior and functionalities emerging from the topological defects, such as skyrmions, multiferroic vortices, domain walls, dislocations, and disclinations [68]. Thus, it is important to characterize domain-defect interactions and their dynamics, as well as to directly link local atomic-displacement to polarization [23,69-73]. Lorentz microscopy has been widely used to study the skyrmions, the magnetic switching and domain configuration evolution. The dynamical process of generation and annihilation of the magnetic biskyrmions have been observed by in situ TEM [72]. As an alternative approach, a dedicated magnetizing stage can be used to generate a magnetic field at the specimen area by adding Helmholtz coils on each side of the specimen for the study of magnetic field induced motion of magnetic domain walls [74,75]. Another possible design is bring the piezo-driven sharp needle made of a permanent magnet close to the specimen [76,77]. To draw the relationship between magnetic structures and temperature, a thermal element also need be integrate with the holder. Meanwhile, a new design capable of applying GHz resonance electric current and pulsed excitations in situ was developed to measure the non-adiabatic spin torque effect [78], and to map strongly coupled coaxial vortex motion in the dipolar- and indirect exchange-coupled regimes [79].

3.1. Ferroelectric vortices

In rare-earth hexagonal manganites $RMnO_3$ (R = Er, Y), vortices and antivortices are topological defects. At high temperature the crystal structure adopts centrosymmetric $P6_3/mmc$. A structural transition occurs at Tc, which lowers the symmetry to $P6_3cm$ mainly by the condensation of the K_3 phonon mode. This process leads to the trimerized tilting of MnO_5 bipyramids and corrugation of intercalated R layers while maintaining the six-fold symmetry with six crystallographically preferred domains denoted as $\alpha+$, $\beta-$, $\gamma+$, $\alpha-$, $\beta+$, $\gamma-$ in sequence around the core [80]. These six-fold vortices are topologically protected and extremely stable under thermal perturbation and external biasing [81-83]. In situ biasing in TEM is the most effective approach to study individual ferroelectric vortex and antivortex formation and inhalation and their dynamic switching behavior. Fig. 4a–c give an example of hexagonal $ErMnO_3$, a geometric ferroelectric since its spontaneous polarization is induced by the structural trimerization of Mn ions and the buckling of Er ions due to mismatch in ionic size between the R-ions and the Mn ions, as shown in Fig. 4c. The symmetry-breaking phase transition of the Mn trimerization engenders two possible directions of polarization along the *c*-axis ("+" being parallel to the *c*-axis, and "−" being antiparallel to it), and three antiphases (α, β, and γ), totaling six distinctive domains ($\alpha+$, $\alpha-$,

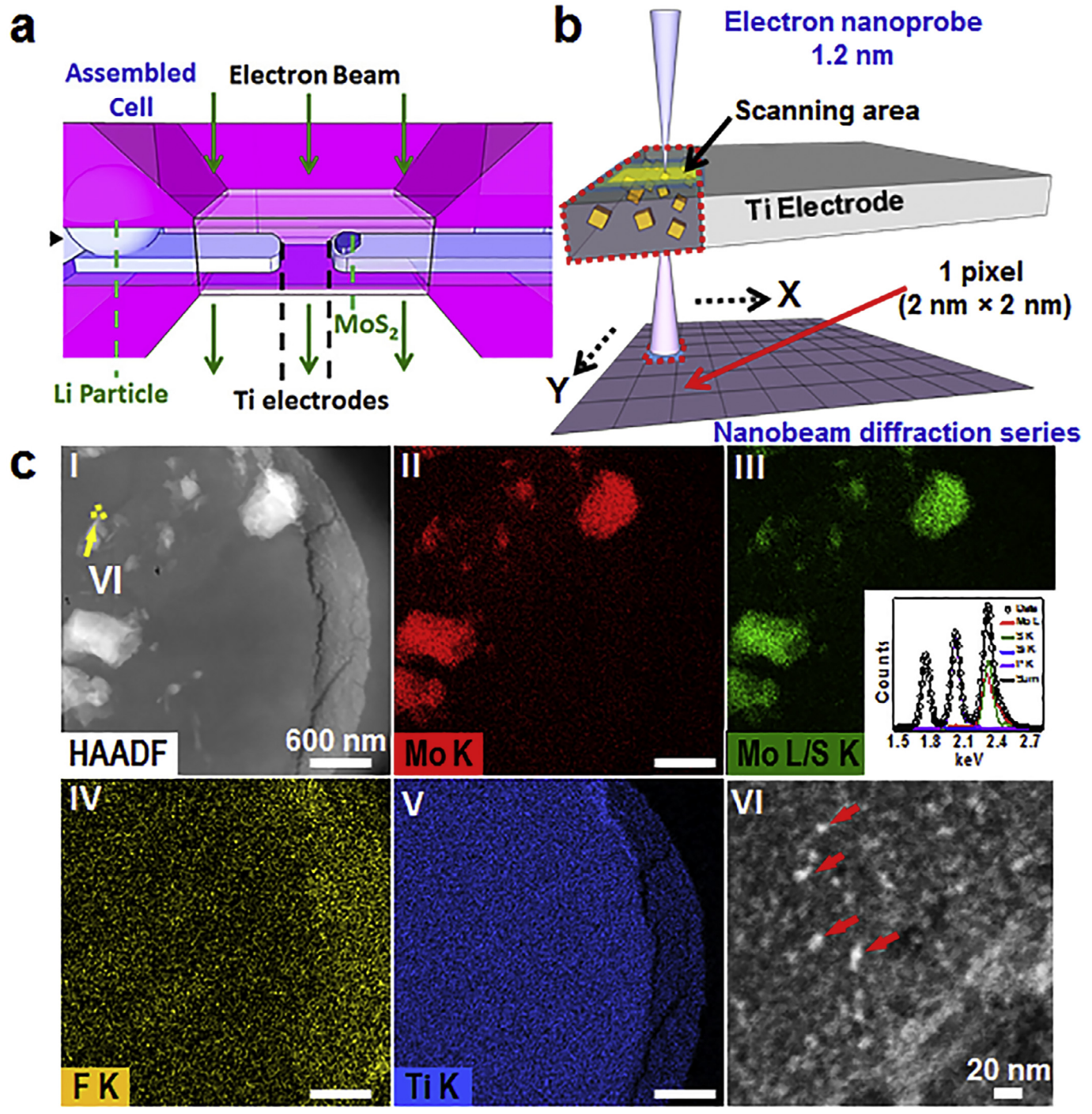

Fig. 3. In situ study of charge-discharge induced electrode structural changes in an electrochemical cell [34]. (a) A home-made electrochemical liquid cell with two Ti electrodes Li and MoS_2 nanoparticles loaded on each side. (b) Integration of the advanced nanobeam diffraction imaging techniques (c). Analysis of Ti electrode with MoS_2 nanoparticles after discharge process. (II-V) EDS mapping showing elemental distribution. Inset in (III) is the quantitative analysis of elements after deconvolution. (VI) Small MoS_2 nanoparticles from nanobeam diffraction imaging in a seemly smooth area of electrode in (I).

$\beta+$, $\beta-$, $\gamma+$, $\gamma-$) [80]. The walls of the trimerization domain, interlocked with ferroelectric domain walls, emerged from topological defects as vortex and antivortex (Fig. 4a) with opposite winding orders. The vortices are quite stable. Even in the presence of severe discontinuities in electric polarization around the core, the formation of these topological defects are observed when the crystal is exposed to temperatures above Tc. There are two types ferroelectric domain walls, type-A and type-B, with lattice shift of 1/3[120] and 2/3[120], across the domain wall, respectively. By measuring the area of polarized domains in situ with applied electric field we can correlate nanoscale polarization to microscale hysteresis property (polarization vs electric field loop) of the sample. For example, when we vary the field from −150 kV/cm (as shown in Fig. 4b) to 150 kV/cm we can direct observe the ferroelectric switching behavior: domains parallel to the field direction expand while those antiparallel to the field direction shrink. Nevertheless, the vortex cores are immobile. We note when two domains are paired they carry opposite charges, resulting in a strong attractive interaction.

Please cite this article as: H. Zheng, Y. Zhu, Perspectives on in situ electron microscopy, Ultramicroscopy (2017), http://dx.doi.org/10.1016/j.ultramic.2017.03.022

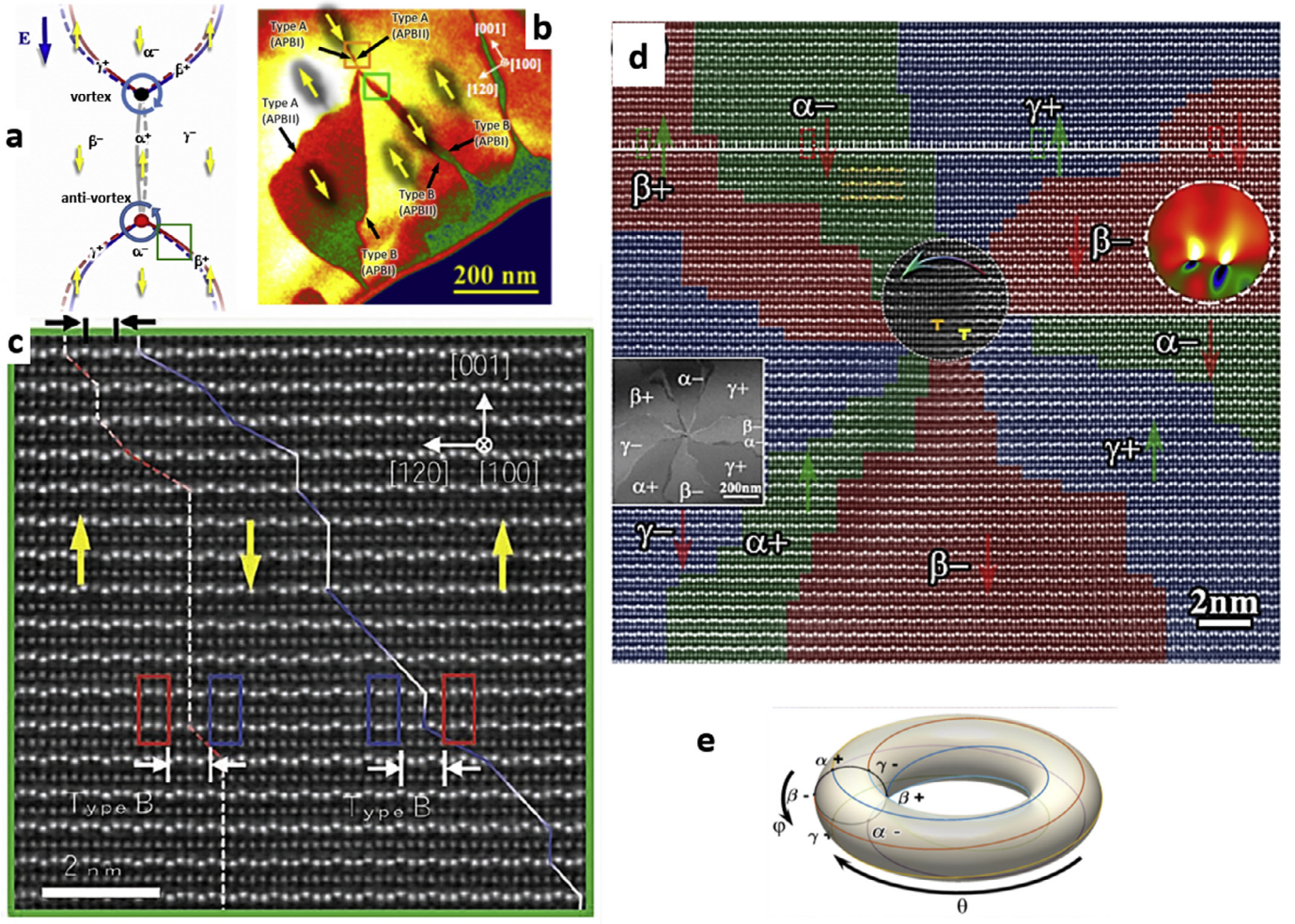

Fig. 4. Ferroelectric vortices. (a) Electrostatic interactions between domain walls around a vortex (black dot)-antivortex (red dot) pair in saturated state under downward applied field. The electrostatic charges associated with the domain walls are marked in red (positive) and blue (negative). When the applied field reverses, the ferroelectric domains with polarization parallel to the field expand while anti-parallel to the field shrink. (b) Dark-field image of a vortex and its associated domains obtained with the 001 reflection in $ErMnO_3$ under applied field of −150 kV/cm, showing domain configuration and different types of domain walls. (c) ADF STEM images from the regions indicated with the green-rectangle in (b). Unit cells for each domain near walls are denoted with blue- and red-rectangles. The two walls highlighted in the high resolution image are type-B walls. Yellow arrows indicate the polarization direction for each domain. (d) An 8-fold vortex in hexagonal $YMnO_3$ in the remnant state observed by atomic resolution dipole mapping. Such a vortex symmetry is crystallographically forbidden but topologically allowed. The vortex core has two edge dislocations associated with it. The inset on the right is the strain map around dislocations near the core and the one on the left shows the corresponding low magnification [80]. (For interpretation of the references to color in this figure legend, the reader is referred to the web version of this article.).

Fig. 4c shows the bound states carrying domains can be as narrow as only 1 unit-cell wide for oppositely charged paired walls, as marked on top left corner of figure. We attribute the stability of these narrow domains to the incommensurability of partial unit-cell-shifts across the paired walls that prevent the unification of the bound states, or pair-annihilating even with one unit-cell separation. It assures the strong short-range repulsive interaction for the bound states. These narrow domains are topologically protected due to the incommensurate sum of the partial unit-cell-shift vectors for each pair of walls, preventing domain annihilation resulting in incomplete polling, a feature that was not observed in stereotypical ferroelectrics, such as $PbTiO_3$ and $BaTiO_3$ [82,84].

Six-fold vortex domains are most common in $RMnO_3$, as they reflect the six crystallographic variants. Non-six-fold vortex domains are inconsistent with the crystal symmetry, thus do not expect to exist in hexagonal manganites. Nevertheless, 2-fold, 4-fold, and 8-fold vortex domains have been recently observed. An example for an eight-fold vortex structures using aberration-corrected electron microscopy is shown in Fig. 4(d), revealing startling detailed atomic configurations of crystallographically forbidden non-six-fold ferroelectric domains surrounding the vortex cores in hexagonal $YMnO_3$. The vortex core is incorporated with two partial edge dislocations (PEDs), another important class of topological defects. The polarization directions of the ferroelectric domains can be distinguished by corrugated configurations of Y-ions, similar to 6-fold vortices. To map the associated strain field of the PEDs of the eight-fold vortex cores, we used geometric phase analyses (GPA) [85], and the strain filed of ε_{xx} (the x axis is defined as the [1 2 0] direction) around the PEDs constructed from the atomic images, as shown in the insets. Clearly, the non-uniform displacement field near the vortex centers (marked by the circles), especially near the PED cores, plays a significant role in altering the corrugated configuration of the vortex structure. The corresponding mesoscale dark-field images that possess dissimilar contrast for oppositely polarized ferroelectric domains due to the breaking of Friedel's law, are also included. Careful atomic image analysis suggests that the PED possesses a Burgers vector of 1/3[120]. To clarify the vortex-forming mechanism, Landau-theory based phenomenological model was used and the origin of the remarkable atomic arrangement and the intertwined relationship between the

Please cite this article as: H. Zheng, Y. Zhu, Perspectives on in situ electron microscopy, Ultramicroscopy (2017), http://dx.doi.org/10.1016/j.ultramic.2017.03.022

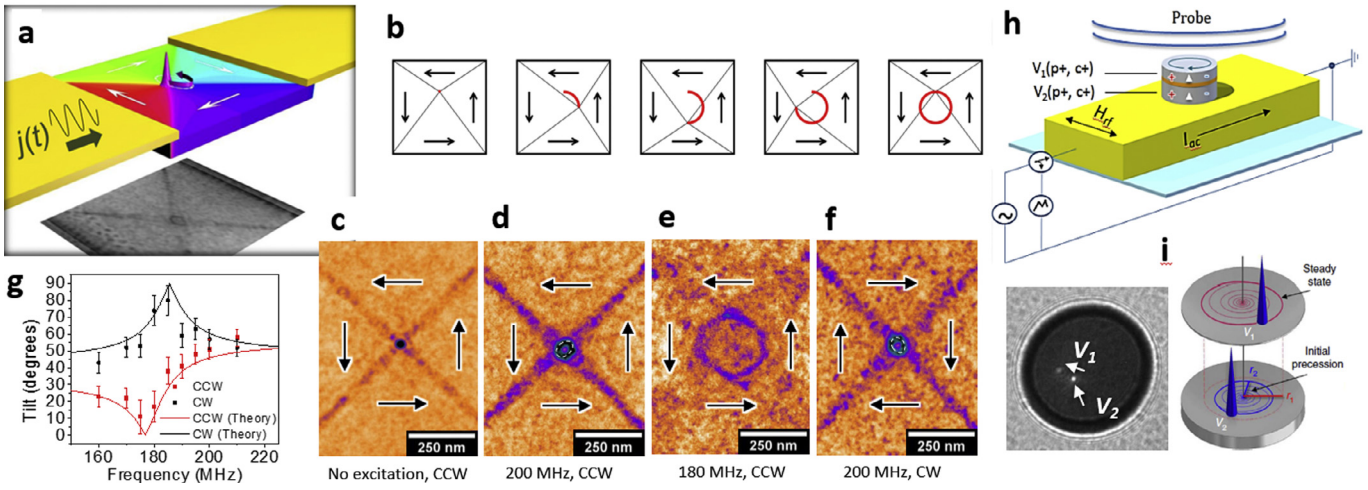

Fig. 5. Ferromagnetic vortices. (a) The vortex precession measurement scheme with in situ high-frequency (subGHz) current excitation. (b) Vortex core precession principle. (c)–(f) Lorentz image of a vortex-core of the Py square Landau structure. (c) Without excitation. The magnetic configuration of the four domains is counter clockwise. (d) Clock-wise (CW) orbit over-, counter CW orbit at-, and CCW orbit over-resonance, showing the evolution of the tilt and orbit amplitude with frequency, and for different chiralities. (g) Orbit tilt vs. frequency. The effects of chirality are subtle, and require high spatial resolution to observe them. (i) Orbit radius vs. current density for both chiralities. The variation can be used to separate Oersted field effects on the orbit, as well as determine the degree of non-adiabaticity associated with spin torques. (g) Measured tilt from the current direction versus frequency for the same element at 7.9×10^{10} A/m^2. The small shift in resonance frequency from that of a current of 1×10^{11} A/m^2 is due to joule heating. (h) A patterned disc heterostructure with a non-magnetic spacer Cu layer sandwiched between two magnetic permalloy layers on top of a Au waveguide and Si_3Ni_4 membrane (not to scale). The tri-layered heterostructure contains two magnetic vortex cores due to the different thickness of the permalloy layer. (i) Lorentz image of the projected in-plane magnetization to capture both vortex cores simultaneously. A schematic of the dissimilar gyrotropic core motion at the respective eigen-frequencies with different radius due to the thickness asymmetry [76].

two types of topological defects, i.e. (anti)vortex cores and partial-edge-dislocations (PEDs), as well as the roles of their displacement field, formation temperature and nucleation sites are revealed. All conceivable vortices in the system are topologically classified using homotopy group theory and their origins are identified. The unanticipated symmetry breaking was found at both mesoscale (domains) and atomic scale (vortex cores) due to the intertwining of two types of topological defects. Due to the interaction of PEDs with surrounding lattice, the initially topologically protected 6-fold (anti)vortex core structures can be transformed into other configurations. Thus, PED, depending on its characteristics, including Burgers vector, formation temperature and nucleation sites, can behave as a control knob for regulating vortex domain symmetry, whatever the methods that could introduce PEDs into this system. The ability to manipulate and control the ferroic orders in RMnO$_3$ in correlation with spontaneous magnetization, electric polarization, and spontaneous strain may provide a platform for exploring emerging physical phenomena with novel applications via topological defects.

3.2. Ferromagnetic vortices

A ferromagnetic vortex is most commonly seen in a magnetic disc or square where in-plan spins circulate form a magnetic vortex at the center with an out-of-plan spin configuration (Fig. 5a). Understanding switching behavior of ferromagnetic nanostructures will enable us to design better spintronic devices. In situ magnetic imaging with Lorentz microscopy has been widely used to study topological defects and quasiparticles, including skyrmions and the evolution of spin structures under magnetic field or electric current. The dynamic switching process of generation and annihilation of spin configurations can be directly observed by applying magnetic field using a sample stage with build-in Helmholtz coils or a piezo-driven magnetic needle, [74,77,86] or by tilting the sample to utilize the magnetic field of the objective lens. A design capable of applying gigahertz resonance electric current and pulsed excitations in TEM was recently developed to measure spin vortex precession orbit and to understand the nonadiabatic spin torque effect [78]. Spin-transfer torque offers great promise for the development of spin-based devices. The effects of spin-transfer torques are typically analyzed in terms of adiabatic and non-adiabatic contributions. Currently a comprehensive interpretation of the non-adiabatic term remains elusive, with suggestions that it may arise from universal effects related to dissipation processes in spin dynamics, and other studies indicating a strong influence from the symmetry of magnetization gradients. The Lorentz microscopy with gigahertz-excitations approach can achieve better than 5 nm spatial resolution to map the orbit of a magnetic vortex core.

Fig. 5a shows a schematic of the spin vortex precession orbit measurement setup. The top corresponds to the sample assembly with its actual Lorentz image at the bottom. A high frequency ac signal is supplied externally through gold contact pads using waveguides to inject high-frequency current. The sample is a permalloy square exhibiting a Landau domain structure with a vertex core in the middle. Fig. 5b illustrates how the vertex core motion forms a vertex-core spin orbit. When a vortex core is displaced from the center of a ferromagnetic disc, the demagnetization energy serves as a restorative force, and the gyrotropic and precessional dynamics can be captured using a harmonic oscillator model. As a result of the core displacement, magnetic 'charges' form on the edges of the disc. These weakly coupled magnetostatic interactions are long range but have a small interaction cross section and even edge overlapped direct exchange discs may demonstrate complex non-linear modes. Alternatively a stacked geometry increases the magnetic interaction over the entire surface areas of the ferromagnetic layers leading to stronger coupling of neighboring vortices.

Fig. 5c–f shows Lorentz micrographs of the vortex core precession orbit at various driving frequencies. The current was applied along the horizontal direction (as marked in Fig. 5a), with the current density maintained at 7.7×10^{10} A/m^2. As the vortex precesses about the central equilibrium point, the domain walls of the Landau structure oscillate about their equilibrium positions, creating blurred domain contrast at their boundaries. The domains, which are pinned by each of the four corners of the spin structure and

the vortex core, move with the vortex core. Imaging of the gyrotropic motion reveals subtle changes in the ellipticity, amplitude and tilt of the orbit as the vortex is driven through resonance, providing a robust method to determine the adiabatic, non-adiabatic spin torque parameters with unprecedented precision. Fig. 5c–e shows the change of vortex-core orbit size of the counter clockwise (CCW) domains, from the remanence (c), off resonance (d, 200 MHz) and at resonance (e, 180 MHz) state, indicating the core reaches maximum at resonance with rather circular orbit. In contrast, as the frequency moves off resonance, the ellipticity of the orbit, which follows an almost linear relationship with the normalized frequency, is clearly visible as illustrated in Fig. 2(d) and (f) for vortices of (polarity = +1, CCW) and (polarity = +1, CW). Fig. 5g depicts the measured tilt from the current direction versus frequency for the same element with a theoretical prediction superimposed (solid line). The measurements of the orbit amplitudes for both chiralities and as a function of frequency allow for the unambiguous determination of the non-adiabatic parameter β and the viscous damping parameter α, respectively. The orbital tilts are sensitive to the relative magnitudes of all three driving contributions: adiabatic, non-adiabatic, and Oersted field contribution. Hence, mapping the tilt angle with respect to frequency allows additional determination of the degree of spin polarization, P, though in practice, local pinning effects can influence low amplitude oscillations and may complicate the measurement of spin polarization.

Another example is direct imaging of mode-coupled magnetic vortices. Interlayer coupled vortices where the magnetic interaction was altered in asymmetric disc heterostructures of Permalloy/Copper/Permalloy Py/Cu/Py). By reducing the non-magnetic spacer layer thicknesses of copper, indirect exchange interactions strongly coupled vortices of non-overlapping eigenmodes, creating spatially coherent core oscillations with a singular peak in the subgigahertz frequency spectrum corresponding to a mode-coupled gyrotropic motion. This is in contrast to the magnetostatic coupled systems where the cores interact in a chaotic manner and the characteristic periodic motion cannot be detected. The coherent oscillations found in the indirect exchange coupled disc heterostructures serves as a basis for more complex coupled systems and could be used as a means of amplification and tuning of the eigenmodes in strongly interacting multi-vortex systems. Fig. 5h shows a schematic diagram of the heterostructures, where the thickness of the two ferromagnetic layers where fixed at 25 nm and 15 nm of Py, separated by a thin Cu layer. At equilibrium, the vortex cores reside in the center of the disc at the energy minimum of the potential landscape. If the two ferromagnetic layers of the device are isolated and excited with an RF field at resonance, the orbital amplitude of the steady state vortex core-path trace (r1, r2) as well as the eigenfrequency ($\omega 1$, $\omega 2$) would be distinct as shown in Fig. 5i. The two vortices can be interpreted as two harmonic oscillators with dissimilar restorative spring constants and masses due to the thickness asymmetry. The non-magnetic Cu layer serves as a means of modifying the interlayer coupling strength. The asymmetry also provides unique behavior as non-overlapping eigenmodes should become evident in the frequency spectrum and can also be used to independently control the states of the vortices. The coherent oscillations found in the indirect exchange coupled disc heterostructures serves as a basis for more complex coupled systems and could be used as a means of amplification and tuning of the eigenmodes in strongly interacting multi-vortex systems. It provides critical insights of the fundamental features of collective vortex-based microwave generators, such as their steady-state amplitudes, tenability and mode-coupled gyrotropic vortex motion. The ability to image coupled multiple vortex cores and excite them into resonant modes has implications for fundamental dynamics of interacting topological defects as well as novel technological utilities, such as magnetic nano oscillators and antennae.

4. Conclusions and outlook

In summary, in situ electron microscopy has attracted broad interest and it has been applied to a wide range of research topics. In this article, two drastically different areas of research that benefit from in situ TEM advancement were discussed. The developments of liquid environmental cells and the advances in electron microscopy such as the aberration corrected optics and fast electron detection have enabled the imaging of materials transformations in liquids with atomic resolution and 2.5 ms temporal resolution. Significant progress has been made in the understanding of colloidal nanocrystal growth with in situ liquid cell TEM. Liquid cell TEM has also been applied to the study of electrochemical processes at electrode-electrolyte interfaces for batteries applications. However, the image resolution for in situ TEM of electrochemical processes in a liquid cell is limited so far, which is partly constrained by electron beam damage. Reducing electron beam effects is crucial for future growth of liquid cell TEM. There is no doubt that liquid cell TEM technologies will experience revolutionary growth in the near future. Breakthroughs are yet to be made on imaging of materials dynamics in liquids with high signal-to-noise ratio, improved spatial and temporal resolution, controlled environments or stimuli and significantly reduced electron beam effects.

Exciting results have also been achieved in the understanding of ferroelectric and ferromagnetic vortex using in situ TEM with the sample stage advancement. The aberration corrected TEM, future improvement of the electron detection technologies and ultrafast electron microscopy development i.e., in μs, ns, ps or fs regime, would allow for exploring more and more atomic level materials dynamics. Ultimately the study of dynamic molecular, atomic events or different phonon modes or transitions in the ultrafast regime with in situ TEM will be enabled.

Acknowledgments

H. Z. thanks her postdocs Hong-Gang Liao, Zhiyuan Zeng and Kaiyang Niu for their contribution to the liquid cell electron microscopy work discussed in this article. She would also like to thank the funding support from U.S. DOE-BES, Materials Science and Engineering Division under contract No. KC22ZH. Y.Z. would like to thank Shaobo Cheng, Jun Li, and Myung-Geun Han for their research on ferroelectric vortices and Shawn Pollard and Javier Pulecio on ferromagnetic vortices. The work at Brookhaven National Lab was supported by the U.S. DOE-BES, Materials Science and Engineering Division, under contract No. DESC0012704.

References

[1] http://science.energy.gov/bes/efrc/research/grand-challenges/.
[2] H.M. Zheng, Y.S. Meng, Y.M. Zhu, *Frontiers of* in situ *electron microscopy*, MRS Bull. 40 (1) (2015) 12–18.
[3] F.M. Ross, Opportunities and challenges in liquid cell electron microscopy, Science 350 (6267) (2015) aaa9886.
[4] H.G. Liao, H.M. Zheng, Liquid cell transmission electron microscopy, in: M.A. Johnson, T.J. Martinez (Eds.), Annual Review of Physical Chemistry, vol. 67, Annual Reviews, Palo Alto, 2016 p. 719-+.
[5] N. de Jonge, M. Pfaff, D.B. Peckys, Practical aspects of transmission electron microscopy in liquid, in: P.W. Hawkes (Ed.), Advances in Imaging and Electron Physics, vol. 186, Elsevier Academic Press Inc, San Diego, 2014, pp. 1–37.
[6] A. Yurtsever, R.M. van der Veen, A.H. Zewail, Subparticle ultrafast spectrum imaging in 4D electron microscopy, Science 335 (6064) (2012) 59–64.
[7] A. Yurtsever, A.H. Zewail, 4D nanoscale diffraction observed by convergent-beam ultrafast electron microscopy, Science 326 (5953) (2009) 708–712.
[8] G.M. Vanacore, A.W.P. Fitzpatrick, A.H. Zewail, Four-dimensional electron microscopy: ultrafast imaging, diffraction and spectroscopy in materials science and biology, Nano Today 11 (2) (2016) 228–249.
[9] Q. Yu, et al., Origin of dramatic oxygen solute strengthening effect in titanium, Science 347 (6222) (2015) 635–639.
[10] Z.W. Shan, et al., Mechanical annealing and source-limited deformation in submicrometre-diameter Ni crystals, Nat. Mater. 7 (2) (2008) 115–119.

Please cite this article as: H. Zheng, Y. Zhu, Perspectives on in situ electron microscopy, Ultramicroscopy (2017), http://dx.doi.org/10.1016/j.ultramic.2017.03.022

[11] C.T. Nelson, et al., Domain dynamics during ferroelectric switching, Science 334 (6058) (2011) 968–971.
[12] L.Z. Li, J.R. Jokisaari, X.Q. Pan, In situ electron microscopy of ferroelectric domains, MRS Bull. 40 (1) (2015) 53–61.
[13] M.D. Rossell, et al., Quantitative Li mapping in al alloys by sub-eV resolution energy-filtering transmission electron microscopy (EFTEM) in the aberration–corrected, monochromated TEAM0.5 instrument, Microsc. Microanal. 15 (2009) 430–431.
[14] H.G. Liao, et al., Real-time imaging of Pt3Fe nanorod growth in solution, Science 336 (6084) (2012) 1011–1014.
[15] E. Michel, H. Ibach, C.M. Schneider, High resolution electron energy loss spectroscopy of spin waves in ultra-thin cobalt films, Surf. Interface Anal. 48 (11) (2016) 1104–1107.
[16] P.E. Batson, N. Dellby, O.L. Krivanek, Sub-angstrom resolution using aberration corrected electron optics, Nature 418 (6898) (2002) 617–620.
[17] D.A. Muller, et al., Atomic-scale chemical imaging of composition and bonding by aberration-corrected microscopy, Science 319 (5866) (2008) 1073–1076.
[18] O.L. Krivanek, P.E. Mooney, Applications of slow-scan CCD cameras in transmission electron-microscopy, Ultramicroscopy 49 (1-4) (1993) 95–108.
[19] Y.M. Bunkov, H. Godfrin, Topological Defects and the Non-Equilibrium Dynamics of Symmetry Breaking Phase Transitions, vol. 549, Springer Science & Business Media, 2012.
[20] T.W. Kibble, Topology of cosmic domains and strings, J. Phys. A: Math. Gen. 9 (8) (1976) 1387.
[21] H.-R. Trebin, The topology of non-uniform media in condensed matter physics, Adv. Phys. 31 (3) (1982) 195–254.
[22] A. Vilenkin, E.P.S. Shellard, Cosmic Strings and Other Topological Defects, Cambridge University Press, 2000.
[23] X. Yu, et al., Real-space observation of a two-dimensional skyrmion crystal, Nature 465 (7300) (2010) 901–904.
[24] H. Das, et al., Bulk magnetoelectricity in the hexagonal manganites and ferrites, Nat. Commun. 5 (2014).
[25] D. Meier, et al., Anisotropic conductance at improper ferroelectric domain walls, Nat. Mater. 11 (4) (2012) 284–288.
[26] W. Wu, et al., Conduction of topologically protected charged ferroelectric domain walls, Phys. Rev. Lett. 108 (7) (2012) 077203.
[27] O. Lavrentovich, Topological defects in dispersed words and worlds around liquid crystals, or liquid crystal drops, Liquid Crystals 24 (1) (1998) 117–126.
[28] M. Fiebig, et al., Observation of coupled magnetic and electric domains, Nature 419 (6909) (2002) 818–820.
[29] F.-T. Huang, et al., Duality of topological defects in hexagonal manganites, Phys. Rev. Lett. 113 (26) (2014) 267602.
[30] L. Marton, La microscopie electronique des objets biologiques, Acad. R. Belgique Bull. Cl. Sci. 20-133 (5) (1934) 439–911.
[31] H.M. Zheng, et al., Observation of single colloidal platinum nanocrystal growth trajectories, Science 324 (5932) (2009) 1309–1312.
[32] H.-G. Liao, et al., Facet development during platinum nanocube growth, Science 345 (6199) (2014) 916–919.
[33] J. Park, et al., 3D structure of individual nanocrystals in solution by electron microscopy, Science 349 (6245) (2015) 290–295.
[34] Z.Y. Zeng, et al., In situ study of lithiation and delithiation of MoS_2 nanosheets using electrochemical liquid cell transmission electron microscopy, Nano Lett. 15 (8) (2015) 5214–5220.
[35] J. Becker, O. Schubert, C. Sonnichsen, Gold nanoparticle growth monitored in situ using a novel fast optical single-particle spectroscopy method, Nano Lett. 7 (6) (2007) 1664–1669.
[36] Y. Sun, Y. Ren, In situ synchrotron x-ray techniques for real-time probing of colloidal nanoparticle synthesis, Particle Particle Syst. Character. 30 (5) (2013) 399–419.
[37] N. Steinfeldt, In situ monitoring of Pt nanoparticle formation in ethylene glycol solution by SAXS-influence of the NaOH to Pt ratio, Langmuir 28 (36) (2012) 13072–13079.
[38] J. Polte, et al., Nucleation and growth of gold nanoparticles studied via in situ small angle x-ray scattering at millisecond time resolution, ACS Nano 4 (2) (2010) 1076–1082.
[39] B. Abecassis, et al., Probing in situ the nucleation and growth of gold nanoparticles by small-angle x-ray scattering, Nano Lett. 7 (6) (2007) 1723–1727.
[40] J. Miao, et al., *Three-dimensional* GaN-Ga_2O_3 *core shell structure revealed by X-ray diffraction microscopy*, Phys. Rev. Lett. 97 (21) (2006) 215503.
[41] G.V. Ramesh, B. Sreedhar, T.P. Radhakrishnan, *Real time monitoring of the* in situ *growth of silver nanoparticles in a polymer film under ambient conditions*, Phys. Chem. Chem. Phys. 11 (43) (2009) 10059–10063.
[42] A.O. Simm, et al., AFM studies of metal deposition: instantaneous nucleation and the growth of cobalt nanoparticles on boron-doped diamond electrodes, ChemPhysChem 7 (3) (2006) 704–709.
[43] A. Kolmakov, D.W. Goodman, In situ scanning tunneling microscopy of oxide–supported metal clusters: Nucleation, growth, and thermal evolution of individual particles, Chem. Record 2 (6) (2002) 446–457.
[44] H.G. Liao, H.M. Zheng, Liquid cell transmission electron microscopy study of platinum iron nanocrystal growth and shape evolution, J. Am. Chem. Soc. 135 (13) (2013) 5038–5043.
[45] L. Manna, E.C. Scher, A.P. Alivisatos, Synthesis of soluble and processable rod-, arrow-, teardrop-, and tetrapod-shaped CdSe nanocrystals, J. Am. Chem. Soc. 122 (2000) 12700–12706.
[46] Y. Yin, A.P. Alivisatos, Colloidal nanocrystal synthesis and the organic-inorganic interface, Nature 437 (2005) 664–670.
[47] H.M. Zheng, et al., *Nanocrystal diffusion in a liquid thin film observed by* in situ *transmission electron microscopy*, Nano Lett. 9 (6) (2009) 2460–2465.
[48] J.W. Gibbs, et al., The Collected Works of J. Willard Gibbs, Longmans, Green and Co, 1902.
[49] G. Wulff, On the question of speed of growth and dissolution of crystal surfaces, Z. Krystallograph. Mineral. 34 (5/6) (1901) 449–530.
[50] Y. Xia, et al., Shape-controlled synthesis of metal nanocrystals: simple chemistry meets complex physics? Angew. Chem. Int. Ed. 48 (1) (2009) 60–103.
[51] N. Tian, et al., Synthesis of tetrahexahedral platinum nanocrystals with high--index facets and high electro-oxidation activity, Science 316 (5825) (2007) 732–735.
[52] C.R. Bealing, et al., Predicting nanocrystal shape through consideration of surface-ligand interactions, ACS Nano 6 (3) (2012) 2118–2127.
[53] E. Ringe, R.P. Van Duyne, L.D. Marks, Wulff construction for alloy nanoparticles, Nano Lett. 11 (8) (2011) 3399–3403.
[54] J.M. Yuk, et al., High-resolution EM of colloidal nanocrystal growth using graphene liquid cells, Science 336 (6077) (2012) 61–64.
[55] W.I. Liang, et al., In situ study of spinel ferrite nanocrystal growth using liquid cell transmission electron microscopy, Chem. Mater. 27 (23) (2015) 8146–8152.
[56] T.J. Woehl, et al., *Experimental procedures to mitigate electron beam induced artifacts during* in situ *fluid imaging of nanomaterials*, Ultramicroscopy 127 (2013) 53–63.
[57] T.J. Woehl, et al., Direct observation of aggregative nanoparticle growth: kinetic modeling of the size distribution and growth rate, Nano Lett. 14 (1) (2014) 373–378.
[58] H.L. Xin, H. Zheng, In situ observation of oscillatory growth of bismuth nanoparticles, Nano Lett. 12 (3) (2012) 1470–1474.
[59] Z.Y. Zeng, et al., In situ TEM study of the Li-Au reaction in an electrochemical liquid cell, Faraday Discuss. 176 (2014) 95–107.
[60] M.H. Sun, et al., Structural and morphological evolution of lead dendrites during electrochemical migration, Sci. Rep. 3 (2013) 3227.
[61] Y.M.A. Wu, et al., In-situ multimodal imaging and spectroscopy of Mg electrodeposition at electrode-electrolyte interfaces, Sci. Rep. 7 (2017) 42527.
[62] Z.Y. Zeng, et al., *Visualization of electrode-electrolyte interfaces in LiPF6/EC/DEC electrolyte for lithium ion batteries via* in situ *TEM*, Nano Lett. 14 (4) (2014) 1745–1750.
[63] T. Stephenson, et al., *Lithium ion battery applications of molybdenum disulfide* (MoS_2) *nanocomposites*, Energy Environ. Sci. 7 (1) (2014) 209–231.
[64] B. Radisavljevic, et al., Single-layer MoS2 transistors, Nat. Nano 6 (3) (2011) 147–150.
[65] Z. Zeng, et al., Single-layer semiconducting nanosheets: high-yield preparation and device fabrication, Angew. Chem. Int. Ed. 50 (47) (2011) 11093–11097.
[66] Z. Zeng, et al., An effective method for the fabrication of few-layer-thick inorganic nanosheets, Angew. Chem. Int. Ed. 51 (36) (2012) 9052–9056.
[67] X.P. Fang, et al., *Mechanism of lithium storage in* MoS_2 *and the feasibility of using Li2S/Mo nanocomposites as cathode materials for lithium-sulfur batteries*, Chem. – Asian J. 7 (5) (2012) 1013–1017.
[68] S. Brazovski, N. Kirova, Theory of plastic flows of CDWs in application to a current conversion, Le J. Phys. IV 9 (1999) (PR10): p. Pr10-139-Pr10-143.
[69] J. Zweck, Lorentz microscopy, in: In-Situ Electron Microscopy, Wiley-VCH Verlag GmbH & Co. KGaA, 2012, pp. 347–369.
[70] L. Huang, M.A. Schofield, Y. Zhu, Control of double-vortex domain configurations in a shape-engineered trilayer nanomagnet system, Adv. Mater. 22 (4) (2010) 492–495.
[71] M. Varón, et al., Dipolar magnetism in ordered and disordered low-dimensional nanoparticle assemblies, Sci. Rep. 3 (2013) 1234.
[72] X. Yu, et al., Biskyrmion states and their current-driven motion in a layered manganite, Nat. Commun. 5 (2014) 3198.
[73] X. Yu, et al., Skyrmion flow near room temperature in an ultralow current density, Nat. Commun. 3 (2012) 988.
[74] A. Budruk, et al., In situ Lorentz TEM magnetization studies on a Fe–Pd–Co martensitic alloy, Acta Mater. 59 (17) (2011) 6646–6657.
[75] A. Kohn, et al., The antiferromagnetic structures of IrMn3 and their influence on exchange-bias, Sci. Rep. 3 (2013).
[76] D. Shindo, et al., Electron holography of Fe-based nanocrystalline magnetic materials, J. Appl. Phys. 95 (11) (2004) 6521–6526.
[77] H. Park, et al., *Direct observation of magnetization reversal in thin* $Nd_2Fe_{14}B$ *film*, J. Appl. Phys. 97 (3) (2005) 033908.
[78] S. Pollard, et al., Direct dynamic imaging of non-adiabatic spin torque effects, Nat. Commun. 3 (2012) 1028.
[79] J. Pulecio, et al., Coherence and modality of driven interlayer-coupled magnetic vortices, Nat. Commun. 5 (2014) 3760.
[80] T. Choi, et al., Insulating interlocked ferroelectric and structural antiphase domain walls in multiferroic $YMnO_3$, Nat. Mater. 9 (3) (2010) 253–258.
[81] J. Li, et al., Homotopy-theoretic study & atomic-scale observation of vortex domains in hexagonal manganites, Sci. Rep. 6 (2016) 28047.
[82] M.G. Han, et al., Ferroelectric switching dynamics of topological vortex domains in a hexagonal manganite, Adv. Mater. 25 (17) (2013) 2415–2421.
[83] J. Li, et al., Ferroelectric annular domains in hexagonal manganites, Phys. Rev. B 87 (9) (2013) 094106.
[84] M.-G. Han, et al., Interface-induced nonswitchable domains in ferroelectric thin films, Nat. Commun. 5 (2014) 4693.
[85] M. Hÿtch, E. Snoeck, R. Kilaas, Quantitative measurement of displacement and strain fields from HREM micrographs, Ultramicroscopy 74 (3) (1998) 131–146.
[86] M.J. Polking, et al., Ferroelectric order in individual nanometre-scale crystals, Nat. Mater. 11 (8) (2012) 700–709.

Please cite this article as: H. Zheng, Y. Zhu, Perspectives on in situ electron microscopy, Ultramicroscopy (2017), http://dx.doi.org/10.1016/j.ultramic.2017.03.022